Advances in Water Resources 159 (2022) 104078

Contents lists available at ScienceDirect

Advances in Water Resources

journal homepage: www.elsevier.com/locate/advwatres

On the influence of river Basin morphology and climate on hydrogeomorphic floodplain delineations

A. Annis [a,*], M. Karpack [b], R.R. Morrison [b], F. Nardi [a,c]

[a] Water Resources Research and Documentation Centre (WARREDOC), Università per Stranieri di Perugia, Perugia, Italy
[b] Department of Civil and Environmental Engineering, Colorado State University, Fort Collins, CO, United States of America
[c] Institute of Water & Environment, Florida International University, Miami, FL 33199, United States of America

A B S T R A C T

Elevation-based hydrogeomorphic models are widely used to parsimoniously delineate floodplains with limited input data using topographic gradients to distinguish floodplain areas from hillslopes. Hydrogeomorphic models generally use scaling laws to assess flood flow depths as a function of contributing drainage areas. Floodplains are consequently mapped as those areas underlying maximum flood levels. Recent scientific literature has demonstrated that hydrogeomorphic models consistently perform from regional to global scale, validating geomorphic floodplain delineations in diverse morphological and hydroclimatic river settings. Nevertheless, the relationship between model fidelity, basin morphology, and basin hydroclimatic conditions is still unclear. Specifically, further investigations on the applicability of scaling laws in semi-arid and low-gradient basins is needed. In this work we investigated how climatic variability and basin slope can influence the parameterization of the abovementioned scaling laws in support of hydrogeomorphic floodplain modeling. Eleven basins in the west-central United States were selected as case studies. This research demonstrated that sub-basins slope and annual rainfall are the most influential morphometric and climatic parameters on scaling law regressions. Specifically, we found that scaling relationships are inconsistent in defining semi-arid basin floodplains (average annual rainfall lower than 570 mm) with low-gradient valley slopes (lower than 5%).

1. Introduction

Floodplain landscape evolution is controlled by a diverse and interlinked set of geologic, geomorphic, and hydrologic processes and conditions (Schumm, 1985). The morphology of alluvial rivers depend on flow variability, sediment supplies, bank vegetation, and the erosivity of underlying geology, while floodplain shaping factors are driven by high-magnitude discharges, erosion and depositional patterns, and river valley confinement (Beechie et al., 2006; Galloway and Hobday, 1996; Gurnell et al., 2012; Montgomery and Buffington, 1997). Furthermore, flow and sediment variability depend on watershed-scale hydrologic patterns, and river gradients are governed by climate, tectonic dynamics, and geological settings. Empirical analyses provide geomorphic and hydrologic thresholds at which river morphology moves from meandering to braided conditions (Knighton and Nanson, 1993; Leopold and Wolman, 1970). And, the evolution of river morphology due to changes in river discharge and sediment load can also be caused by legacy of watershed and river alterations (Wohl et al., 2017) and ongoing changes in climate (Hickin, 2009).

The spatial and temporal evolution of river patterns, largely due to water-driven erosion and deposition processes occurring for thousands of years, results in a floodplain geomorphic footprint that can be extracted from topographic datasets, such as Digital Elevation Models (DEMs). As the spatial resolution and accuracy of DEMs have increased, several DEM-based hydrogeomorphic models have been proposed for capturing the floodplain extension as natural landscape features (Dodov and Foufoula-Georgiou, 2006; Jafarzadegan and Merwade, 2017; Manfreda et al., 2014, 2015; Nardi et al., 2006; C. Samela et al., 2017b; Sangwan and Merwade, 2015; Sechu et al., 2020). Some of these approaches (Manfreda et al., 2015; Nardi et al., 2006, 2013; C. Samela et al., 2017b) employ scaling laws that relate channel geometry (depth and width) to discharge (Leopold and Maddock, 1953) or to contributing area (Dodov and Foufoula-Georgiou, 2004a). Scaling laws have been also investigated to hold for overbank flow conditions, being validated to support floodplain hydraulic geometry analyses (Bhowmik, 1984; Nardi et al., 2006). These hydrogeomorphic approaches have been applied at basin (Annis et al., 2019; Nardi et al., 2013; F. 2018; C. Samela et al., 2017b), continental (C. Samela et al., 2017a) and global (Di Baldassarre et al., 2020; Nardi et al., 2019) scales.

Hydrogeomorphic floodplain delineation approaches do not require the estimation of flood hydrographs and detailed surveyed cross sections, and instead require only DEMs that are widely available globally

* Corresponding author at: WARREDOC, Università per Stranieri di Perugia: Universita per Stranieri di Perugia, Piazza Fortebraccio 4, 06123 Perugia, PG, Italy.
E-mail address: antonio.annis@unistrapg.it (A. Annis).

https://doi.org/10.1016/j.advwatres.2021.104078
Received 14 July 2021; Received in revised form 14 October 2021; Accepted 12 November 2021
Available online 18 November 2021

at different resolution and accuracy. Therefore, hydrogeomorphic approaches are less sensitive to data scarcity and are more computationally efficient compared to hydraulic modeling. However, hydrogeomorphic floodplain delineation approaches are not always defined based on a specific flooding recurrence interval and do not take in to account the role of hydraulic structures and climate change because they are conceptualized to delineate natural landscape features that have been historically shaped by the accumulated effects of floods of varying magnitudes (Di Baldassarre et al., 2020). Therefore, in lieu of identifying flood hazard areas for policy purposes, hydrogeomorphic floodplain datasets can be adopted to quantitatively assess anthropogenic effects on natural floodplain environments, such as evaluating for impact of levees on wetlands (Morrison et al., 2018) or investigating floodplain connectivity patterns (Scheel et al., 2019). Moreover, their computational efficiency and parsimony in terms of requested input data allow them to easily delineate floodplains of secondary river networks with greater coverage even in data scarce regions.

River basin morphology, and specific landscape parameters such as channel slope, hypsometric curve, valley confinement, and upstream channel initiation, can influence how hydrogeomorphic models identify floodplain areas. For example, C. Samela et al., 2017b determined different threshold values of their Geomorphic Flood Index for flat versus hilly basins. Annis et al., 2019 identified optimal scaling parameters for a hydrogeomorphic model by considering both DEM resolution and stream order hierarchy, which is related to river basin morphometry. However, since low-order streams can also occur in the lower basin domains, (e.g. small tributaries in flat areas close to the river mouth) it was found that a morphology-driven scaling law parameterization based only on stream orders would not properly estimate floodplains along flat downstream small tributaries. Investigations in Annis et al., 2019 suggest that scaling law parameter regionalization should also consider climate drivers and, in particular, interdependencies of climatic variability with hydrogeomorphic forcing parametrizations. Studies on the impacts of integrated hydrogeomorphic and climate variability on floodplain delineations are sparse.

Climatic conditions have a strong influence on the applicability of hydraulic geometry scaling laws at floodplain scales. Scaling relationships using contributing areas (A) as morphometric descriptor of channel flow depths (d) and channel width (W) (hereafter referred to as d-A and W-A relationships) tend to be subject of significant uncertainties when used to assess out-of-banks floodplain flow levels. In humid environments, channel dimensions tend to increase with contributing area, such that downstream river segments are larger and convey more flow compared to upstream sections (Dodov and Foufoula-Georgiou, 2005; Ferguson, 1986; Knighton, 2014). Semi-arid and arid regions are more prone to have ephemeral rivers whose widths can oscillate, decrease (Dunkerley, 1992), or reach asymptotic values (Knighton and Nanson, 1993; Tooth, 2000). For example, in arid Australian rivers, Tooth (2009) observed a decrease in channel width as contributing areas increased in relatively small rivers, but in larger rivers the relationship between channel width and contributing area was not consistent due to geological discontinuities. Merritt & Wohl (2003) observed that channel widths in an ephemeral arid stream were most sensitive to precipitation regimes as compared to channel depths.

Furthermore, the channel hydraulic geometry and floodplain areas are difficult to define in semi-arid and arid environments (Bourke and Pickup, 1999). In low-gradient dryland rivers, well-defined floodplains may be entirely absent (Tooth, 2000). And, in braided channel systems, floodplains may exist as areas above low terraces (Graf, 1988) or undefined zones adjacent to the channel characterized by a composite mixture of alluvial features (Parsons, 1994).

We believe there is a research gap in the quantitative estimation of scaling law parameters for large scale floodplain delineation based on varying climate and river basin morphometry. In fact, current continental or global hydrogeomorphic floodplain datasets provide constant power laws parameters regardless the abovementioned factors that influence the floodplain morphology. Therefore, this work seeks to address this challenging knowledge gap and, more specifically, seeks to quantify the ranges of validity of d-A relationship parameters for producing consistent floodplain delineations when applied in varying morphologic and climates regimes. In this study we identify the morphometric and climatic attributes of a basin that most influence d-A relationships for floodplains in semi-arid and arid river systems. Unlike other studies focused on developing very accurate and high resolution floodplain datasets from lidar data (Clubb et al., 2017; Stout and Belmont, 2014), this work is focused on providing ranges of d-A scaling laws parameters for continental/global-scale floodplain datasets. The results of this work support the refinement of the hydrogeomorphic floodplain identification method developed by authors, GFPLAIN dataset and algorithm (Annis et al., 2019; Nardi et al., 2019), by means of a novel regionalized application of scaling law parameters that reflect classified geomorphic and hydrologic conditions. We used eleven river basins located in the central Unites States as case study basins.

2. Study basins and available data

We analysed eleven neighbouring river basins located in the states of Colorado, Kansas, Nebraska, New Mexico, Oklahoma, Utah and Wyoming, USA (Fig. 1), which we selected because of their significant variability in morphology and climate. The basins are defined by the boundaries of their 2-digit Hydrologic Unit Codes (HUC-2) (Seaber et al., 1987). The total area of the adjoining basins is approximately 790,960 km^2. Selected climatic and morphometric parameters of the study basins are reported in Table 1, and include basin areas, elevation ranges, slopes, and average annual rainfall. In addition, the basins' hydrologic monitoring network include a total of 583 U.S. Geological Survey (USGS) stage gages (Fig. 1). The rivers of the eastern, arid basins of study area experience large seasonal discharge fluctuations due to snow melt, infiltration, and evaporation losses. The selected study domain is, thus, expected to be characterized by a complex set of large scale meteo-climatic and tectonic changing dynamics interplaying with varying local geomorphic and hydrologic conditions to influence the floodplain and river geometry. Moreover, significant human alterations to the watersheds and rivers have occurred in large portions of the study basins (Nadler and Schumm, 1981), including agriculture land use changes and irrigation diversions, causing increased return flow, higher water tables, and the transformation of some rivers from intermittent to perennial systems (Lurtz et al., 2020). These hydrologic alterations have led to dramatically changing floodplain vegetation and surface water patterns (Nadler and Schumm, 1981) and could influence the scaling law parameterization in the selected study area. However, since river alterations are globally widespread (Döll et al., 2009) this work constitutes an opportunity to test the effectiveness of scaling laws in river basins with human alterations.

2.1. Topography, rainfall, and temperature data

We used the NASADEM dataset (Crippen et al., 2016) at 1 arc resolution (equivalent to approximately 28.8 m projected to the North American Datum of 1983 Universal Transverse Mercator 13 North - NAD83-UTM13N). NASADEM reprocessed the original SRTM radar signal and telemetry data with updated algorithms and auxiliary data not available at the time of the original SRTM processing. Among the globally freely available DEMs, the NASADEM represents one of the most accurate high resolution topographic dataset available to date. The USGS's High Resolution National Hydrography Dataset (NHDPlus) was used to recondition the DEM avoiding potential stream network mapping artefacts due to flat areas or DEM hydrologic impurities (e.g. internal outlets, planar slopes, parallel channels).

We used the PRISM Climate Group's average annual rainfall dataset characterized by ~865 m of horizontal spatial resolution for the 30-year period between 1981 and 2010 (Daly and Bryant, 2013) for average

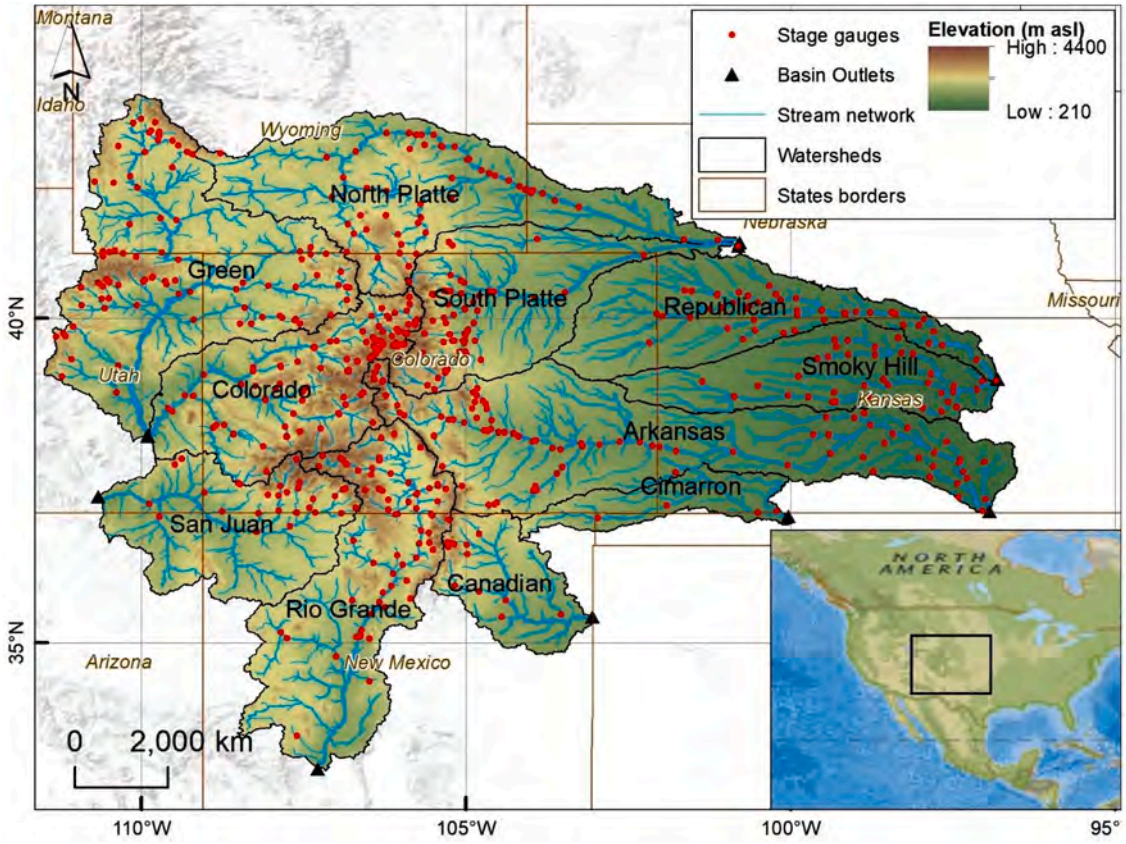

Fig. 1. Map of the study area: major river basins of west-central United States of America. Source data: Stage Gauges from U.S. Geological Survey (USGS); Basins elevations from NASADEM (Crippen et al., 2016); Stream network and watersheds extracted from NASADEM.

Table 1
. Morphometric and hydrologic parameters of the study basins.

Basin name	Area (km^2)	Elevations (m asl) Min.	Max.	Mean	Mean slope (%)	Average Annual rainfall (mm)
Arkansas	122,419	291	4388	1297	7.20	524.2
Canadian	32,431	1069	4160	1804	9.90	452.6
Cimarron	21,858	612	2683	1165	4.99	454.2
Colorado	67,995	1102	4359	2448	23.72	539.6
Green	116,110	1131	4178	2164	15.57	397.4
North Platte	89,156	855	3934	1891	8.00	396.5
Republican	64,676	287	1818	962	4.41	531.8
Rio Grande	91,171	1264	4314	2241	13.42	400.2
San Juan	63,578	1081	4250	1994	13.67	347.1
Smoky Hill	51,771	283	1471	689	4.54	611.1
South Platte	61,973	850	4332	1818	9.04	445.4

annual rainfall to each basin.

The basins are characterized by elevations ranging from 200 to 4400 m above sea level (m asl). The NASADEM-derived basin slope (%) and average annual rainfall (mm) variables are shown respectively in Fig. 2a) and b). The largest basin slopes and average annual rainfall observations are located in the central-west part of the study area, corresponding to the Rocky Mountains. The areas surrounding the Rocky Mountains are relatively dry, while higher an average rainfall is observed in the eastern part of the study domain.

We also used the global aridity index dataset (Trabucco, A., and Zomer, A. 2018; Zomer et al., 2008) for the 1970–2000 period to characterize climatic variability in the basins. The global aridity index is calculated as *P/PET*, where *P* and *PET* are the mean annual precipitation and the potential evapotranspiration (UNEP, 1997; Zomer et al., 2008). Fig. 2(c) shows a wide variability of the aridity index in the study area, where the Rocky Mountain region and the eastern portion of the study area are classified as sub-humid to humid, and the areas surrounding the Rocky Mountains vary from semi-arid to arid.

3. Methodology

This section depicts the methodology adopted in this study including preliminary steps for: estimating the 100-years flood stages (Section 3.1.1) and the DEM pre-processing procedure (Section 3.1.2). Then, the methods employed to identify the morphological and climatic parameters that may have stronger influence on *d-A* relationship performances in each basin (Sections 3.2 and 3.3). Thus, an assessment method is described to evaluate the suitability of *d-A* scaling relationships to identify floodplains in basins with various ranges of climatic and geomorphic conditions (Section 3.4), and the procedure implemented for improving the application of the selected hydrogeomorphic floodplain identification model (Section 3.5). A general schematic flowchart of the entire methodology employed in this work is depicted in Fig. 3.

3.1. Preliminary steps

3.1.1. Estimation of the flood stages at USGS gages

We performed flood frequency analyses using discharge observations from USGS gages within each HUC-2 basin to estimate the 100-year flood flow following the procedures outline in Bulletin 17C (U.S. Water Resources Council. Hydrology Committee, 1981). We used data from gages that contained more than 30 years of records, filtering out gages that did not contain peak annual data and flow records that had error codes. To obtain the flood stage corresponding to the 100-year flood event, the annual peak discharge and stage data reported for

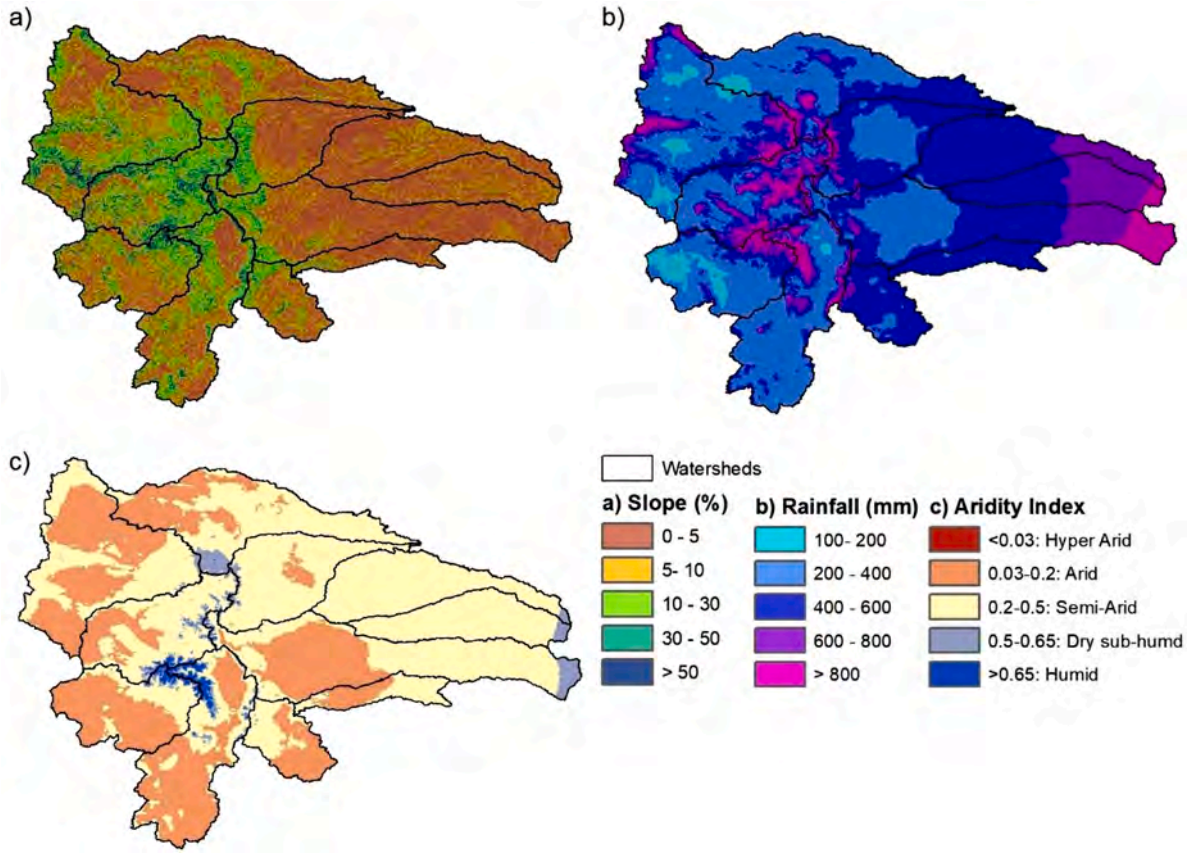

Fig. 2. Maps of slopes (a), average annual rainfall (b), and Aridity Index (c) for the study basins.

each gage was used to create a rating curve for each gage. Different regression distributions and a non-parametrized generalized additive model (GAM, Hastie and Tibshirani, 1990) were fitted to these historical stage and discharge data so that the rating curve could be used to compute stage for any given discharge, including extrapolating above observed values. We found that the GAM fitting method produced a higher Nash Sutcliffe efficiency for almost all gages. Additionally, a visual inspection showed that the GAM caught the breaks in slope of stage-discharge curves more accurately than parameterized models, such as Generalized Extreme Value (GEV) regressions. A total of 570 gages were used for this study (see Supplementary Material for detailed information on the selected USGS gages for each study basin). Note that almost every gage can be influenced by at least one weir or dam located in the upstream drainage area.

3.1.2. DEM pre-processing

We reconditioned the NASADEM by means of the NHDPlus high-resolution stream network dataset using the ArcHYdro toolbox. We derived a dataset of stream networks within each basin by applying pit-filling, flow direction and flow accumulation algorithms (Jenson and Domingue, 1988) to the reconditioned NASADEM dataset. Following the criterion proposed by Annis et al., 2019, we chose a threshold area for the stream network extraction equal to 10 km^2 for the 28-m cell sized NASADEM. For each USGS gages, basins and sub-basins and their related morphometric and climatic parameters were delineated according to the methodology illustrated in Section 3.3.

3.2. Regression analysis of the d-A scaling laws for each basin

We represented 100-years flow depth gradients along the stream network (produced during the DEM pre-processing step described in Section 3.1.2) using a scaling law that relates contributing area (A) to flow depths (d) (Dodov and Foufoula-Georgiou, 2004b; Leopold and Maddock, 1953). As shown in the Eq. (1), this relationship includes parameters a and b, which we determined by using flow depths and contributing areas at USGS gages within each HUC-2 basin (Nardi et al., 2006; F. 2018).

$$\mathrm{d} = aA^b \tag{1}$$

3.3. Analysis of the most influential morphometric and climatic parameters on the d-A scaling law

To evaluate the impact of basin morphology and climate on the *d-A* scaling relationships, we determined different morphometric and climatic characteristics (see Table 2) for each drainage area contributing to each of the 570 stage gages considered in the study area. Some of the characteristics reported in Table 2 are related to an entire HUC-2 basin, while others are related to the partial sub-basins created by gages located within each HUC-2. We defined a sub-basin as the drainage area associated with a particular gage excluding the drainage areas of other gages located upstream. Note that basins and sub-basins are coincident where gages do not have other stage gages in their upstream drainage areas. We sorted the 570 gages into classes (bins) according to each of the above-mentioned characteristics, with equal numbers of sub-basins in each. The number of classes were varied from 3 to 6, such that the minimum number of gauges per bin varies from 55 (6 bins) to 110 (3 bins).

We developed power regressions of *d-A* scaling relationships for each bin according to Eq. (1). We evaluated the fit of each regression using coefficient of determination values (R^2), and we assessed the Pearson correlation between morphometric and climatic characteristics and*d-A* regression fits by using R^2 values. Furthermore, we tested the sensitivity of bin sizing on changes the correlations between the fit of *d-A*

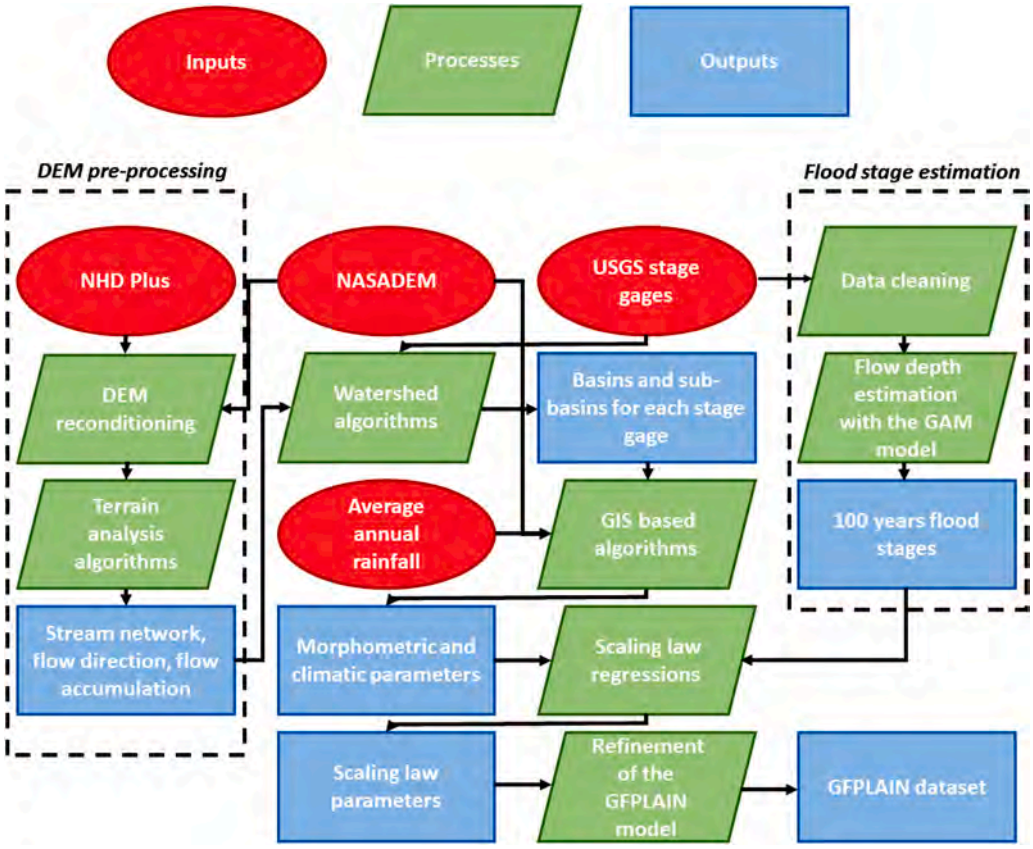

Fig. 3. Flowchart of the methodology.

regression fits and different morphometric and climatic variables.

3.4. Scaling law regression analysis with varying morphometry and climate characteristics

After determining the appropriate scaling parameters to use in *d-A* scaling functions according to differences in basin morphometric and climate characteristics, we evaluated the scaling functions along different Strahler stream order hierarchies. Specifically, we used Pearson correlation coefficients, standard deviation errors and p-values (with a significance level of 0.05) to relate the log-log linear regression to varying morphometric and climatic characteristics within each stream order.

3.5. Development and application of a modified hydrogeomorphic floodplain delineation model

We explored whether the hydrogeomorphic floodplain identification algorithms (Nardi et al., 2006) can be improved by using updated scaling parameters (a and b from Eq. (1)) for different ranges of morphometric and climate characteristics. Specifically we chose to evaluate the GFPLAIN algorithm developed by Nardi et al., 2006 and simplified by Nardi et al., 2013, F. 2018. In the GFPLAIN model, the scaling laws are applied in GIS environment to each flow accumulation cell belonging to the stream network delineated as illustrated in Section 3.1.2. Then, the water level derived by the scaling law is used to flag as floodplain all the low-lying cells of the basin hydrologically connected to the abovementioned channel cell (Nardi et al., 2019). Note that the difference between the river bed elevation and the DEM-derived elevation at the stream network is neglected, since the purpose of the GFPLAIN model is not to replicate the same extension of the 100-years flood hazard maps, but to have consistent scaling law parameters across varying climatic and morphometric basin settings. This implies that the width of the hydrogeomorphic floodplain is usually wider than flood hazard maps, especially because flood control structures are usually not included in current global DTMs. Previous scientific studies applied the GFPLAIN algorithm across a wide range of varying morphological and climatic conditions with fixed scaling law parameters, and obtained consistent results as compared to standard flood hazard maps (Nardi et al., 2019; Di Baldassarre et al., 2020).

We compared the performance of the GFPLAIN algorithm with updated scaling parameters to the original GFPLAIN model using the Critical Success Index (CSI) and the True positive Rate using as reference the FEMA flood maps (https://www.fema.gov/flood-maps) in the study area. These maps can be considered as an official dataset of floodplain extension related to a specific probability of occurrence, and therefore can be considered a good reference for our proposed hydrogeomorphic floodplain dataset.

4. Results

4.1. Regression of the d-A relationships

Log-log regression plots of *d-A* relationships in each basin are reported in Fig. 4 and show that scaling law relationships widely vary among the basins. All the basins with significant coefficient of determination values (R^2) show a positive trends in the *d-A* relationship, while other basins with flat (e.g. North Platte and Smoky Hill) or negative (Republican) curve are not significant in terms of R^2 coefficient. All regression results are statistically significant based on a p-value of 0.05 except for Cimarron, North Platte, Republican and Smoky Hill basins (see Table SM1 of the Supplementary Material). This indicates that increases in drainage contributing areas do not always correlate with an increase of flow depths. This is consistent with the

Table 2
List of morphometric and climatic parameters considered for deriving the d-A regression laws among different parameters' ranges. Each parameter is related to the drainage area of each stage gage. Morphometric dataset are derived by the NASADEM (Crippen et al., 2016) terrain analysis. Climatic variables are derived from PRISM dataset (Daly and Bryant, 2013).

Code	Variable name	Definition	Reference
STO	Stream Order (Strahler)	Numerical measure of river's branching complexity at the stage gage	Strahler, 1952
CAR	Contributing area (km^2)	Drainage area of the basin	Strahler, 1952
PSL	Partial slope (%)	Slope of the sub-basin	Miller and Summerson, 1960
TSL	Total slope (%)	Slope of the basin	Miller and Summerson, 1960
PAR	Partial Average Annual Rainfall (mm)	Average Mean Annual Rainfall of the sub-basin	Chorley, 1957
TAR	Total Average Annual Rainfall (mm)	Average Mean Annual Rainfall of the basin	Chorley, 1957
MFL	Maximum flow length (km)	Length along the longest watercourse from the stage gage position to the watershed limits	Mueller, 1968
PBR	Partial basin relief (m)	The elevation difference between the highest point on the sub-basin drainage divide and the stage gage position	Costa, 1987
TBR	Total basin relief (m)	The elevation difference between the highest point basin drainage divide and the stage gage position	Costa, 1987
TSN	Total stream number	Number of the basin's stream segments	Horton, 1945
TCL	Total channel length (km)	Maximum Length of the channel from the stage gage	Chow, 1965
PCS	Partial channel slope (%)	Channel slope in the sub-basin	Costa, 1987
TCS	Total channel slope (%)	Channel Slope in the basin	Costa, 1987
TDD	Total drainage density (1/km)	Ratio between the total streams' length and the upstream basin contributing area	Gregory and Walling, 1968
PSI	Partial sinuosity index	Ratio between the sub-basin's channel length and the valley length (i.e. the straight distance from the stage gage and the farthest channel point inside the sub-basin)	Wolman and Miller, 1960
TSI	Total sinuosity index	Ratio between the basin's channel length and the valley length (i.e. the straight distance from the stage gage and the farthest channel point inside the upstream basin)	Wolman and Miller, 1960
TFF	Total basin form factor	Ratio between contributing Area and basin length	Horton, 1932
TCR	Total basin circularity ratio	4π (CAR)/P^2 where P is the basin perimeter	Miller and Summerson, 1960
TCC	Total Compactness coefficient	0.2841 P/($CAR^{0.5}$)	Gravelius, 1914
TFR	Total Fitness ratio	Ratio between maximum flow length and basin perimeter	Melton, 1957

climatic and morphometric nature of the selected non-Hortonian basins.

4.2. Sensitivity of regression analysis to sub-basins' morphometric and climatic parameters

We assessed correlations between various morphometric and climatic variables and the overall fit of *d-A* scaling relationships using R^2 calculations, as illustrated in Section 3.2. Fig. 5 shows the R^2 correlations between each variable and the fit of *d-A* regressions using equally sized bins of sub-basins (varied between three and six) according to their corresponding ranges of morphometric and climatic variables. The partial slope (PSL; $0.657 < R^2 < 0.961$) and total basin circularity ratio (TCR; $0.772 < R^2 < 0.963$) are the morphometric variables that have the strongest influence on the fit of *d-A* regressions, while the Partial Annual Rainfall (PAR; $0.771 < R^2 < 0.968$) is the most correlated climatic variable to the fit of *d-A* regressions.

Because PSL, PBR and TCR are strongly correlated to each other (see correlation matrix in Figure SM2 of the Supplementary Material) the PSL of a sub-basin can serve as a single reference morphometric parameter for differentiating *d-A* scaling relationships. Likewise, the PAR can serve as a single reference climatic parameter for differentiating *d-A* scaling relationships within a sub-basin. Note that sub-basins have a minimum partial contributing area of 10 km^2, therefore PSL and PAR can be considered representative variables of at least the lower portion of each sub-basin near gage locations.

4.3. Regression analysis varying slope ranges

The strength of *d-A* scaling relationships varied for different ranges of sub-basin slopes (Fig. 6). The linear correlation of *d-A* relationships strengthens as sub-basin slopes increase, with R^2=0.008 for slopes between 2 and 5% and R^2=0.626 for slopes between 26 and 56%. Similar results were obtained considering the TSL instead of the PSL (See section 1.6 of the Supplementary material). These results confirm that higher energy gradients tend to increase the flow peak and the water level with the increasing of contributing areas. Fig. 7 shows increasing of Person's correlation coefficient related to the *d-A* regressions, and the corresponding decreasing of standard deviation errors with increasing slope. The *d-A* regression for the lowest slope range is not statistically significant according to the p-value test at 0.05 level (see Table SM 2 in the Supplementary Material). In addition, the slope of the *d-A* relationship decreases as sub-basin slope also decreases (represented by the *b* parameter values in Fig. 7), indicating lower correlations between contributing areas and flow depth as average slope decreases.

We further analysed differences in *d-A* relationships across sub-basin slopes using the heat maps of variable slope ranges (Fig. 8). P-values (Fig. 8b) close to the northwest-southeast diagonal are close or higher than 0.05 because of the small sample size (Fig. 8a) and should not be considered in the analysis. It is clear that R^2 (Fig. 8c) and standard deviations (Fig. 8d) tend to increase and decrease at both the lower and higher slope range thresholds.

4.4. Regression analysis varying slope and rainfall ranges

The *d-A* scaling relationships were found to slightly improve when considering higher ranges of average annual precipitation. Fig. 9 shows heat maps of correlation coefficients (top left panel) and standard deviations (top right panel) of *d-A* regressions for a range of sub-basin slope-rainfall combinations. At higher slope ranges, where *d-A* regressions are strongest, correlation coefficients generally increase and standard deviation errors generally decrease with increasing rainfall values, though exceptions are noted, such as the values related to the 16–26% and 439–574 mm ranges of sub-basin slope and annual rainfall. On the other hand, similar patterns are not evident in flat areas (slopes < 5%), where *d-A* regressions perform poorly regardless the annual rainfall of the basins. This is also confirmed by the lower panels of Fig. 9, which shows that *b*-parameters increase (bottom right panel) and *a*-parameters decrease (bottom left panel) with increasing average annual rainfall, particularly for slopes greater than 5%. Moreover, regression analyses for slopes greater than 16% are statistically significant according to their related p-values (Table SM 3).

Fig. 10 shows how regression performances vary after changing the

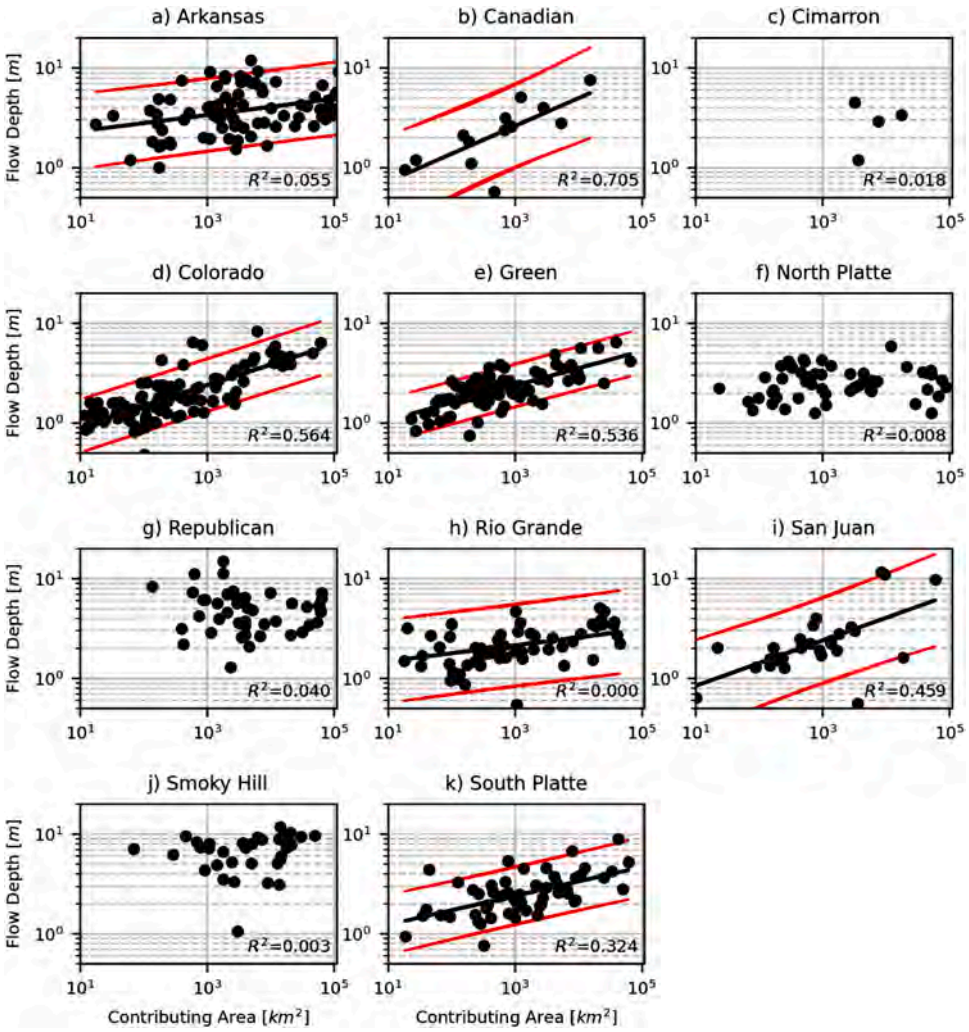

Fig. 4. Regression plots of the contributing area versus the 100-year flood stages in each basin. Each circle represents the flow depths obtained from the methodology illustrated in Section 3, the black lines represent the regression of the scaling law $\boldsymbol{d = aA^b}$, red lines are 90% confidence intervals of the regression. Regression lines and confidence intervals are not reported for basins with not significant regressions (p-value > 0.05).

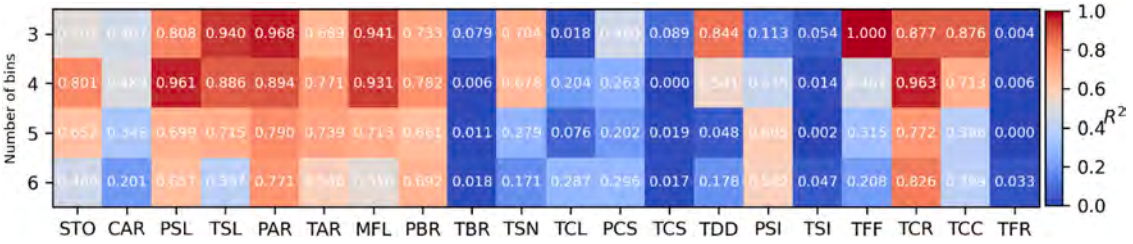

Fig. 5. Heatmaps of R^2 values between the ranges of the parameters listed in Table 2 and the Pearson correlation of the d-A scaling law varying the number of bins from 3 to 6. Ranges are calculated to have equal numbers of sub-basins in each bin. Acronyms of the parameters are: STO:Stream Order (Strahler); CAR:Contributing area (km2); PSL:Partial slope (%); TSL:Total slope (%); PAR:Partial Average Annual Rainfall (mm); TAR:Total Average Annual Rainfall (mm); MFL:Maximum flow length (km); PBR:Partial basin relief (m); TBR:Total basin relief (m); TSN:Total stream number; TCL:Total channel length (km); PCS:Partial channel slope (%); TCS: Total channel slope (%); TDD:Total drainage density (1/km).

lower limits of sub-basin slopes and rainfall ranges in the sample. Values of R^2 (Fig. 10c) and standard deviations (Fig. 10d) tend to improve when both the lower slope and rainfall thresholds are increased, thus confirming that sub-basin average rainfall influences the effectiveness of the *d-A* regressions regardless of the sub-basin slopes.

4.5. Regression analysis varying Strahler stream orders

We also considered the role of Strahler stream orders in the variability of *d-A* regression fits within the basins by using disparate slope and rainfall ranges for each stream order (Fig. 11). We considered only two slope and rainfall ranges for each stream order to maintain larger sample sizes of each regression, Fig. 11 shows that correlation coefficients and standard deviation errors generally improve for larger

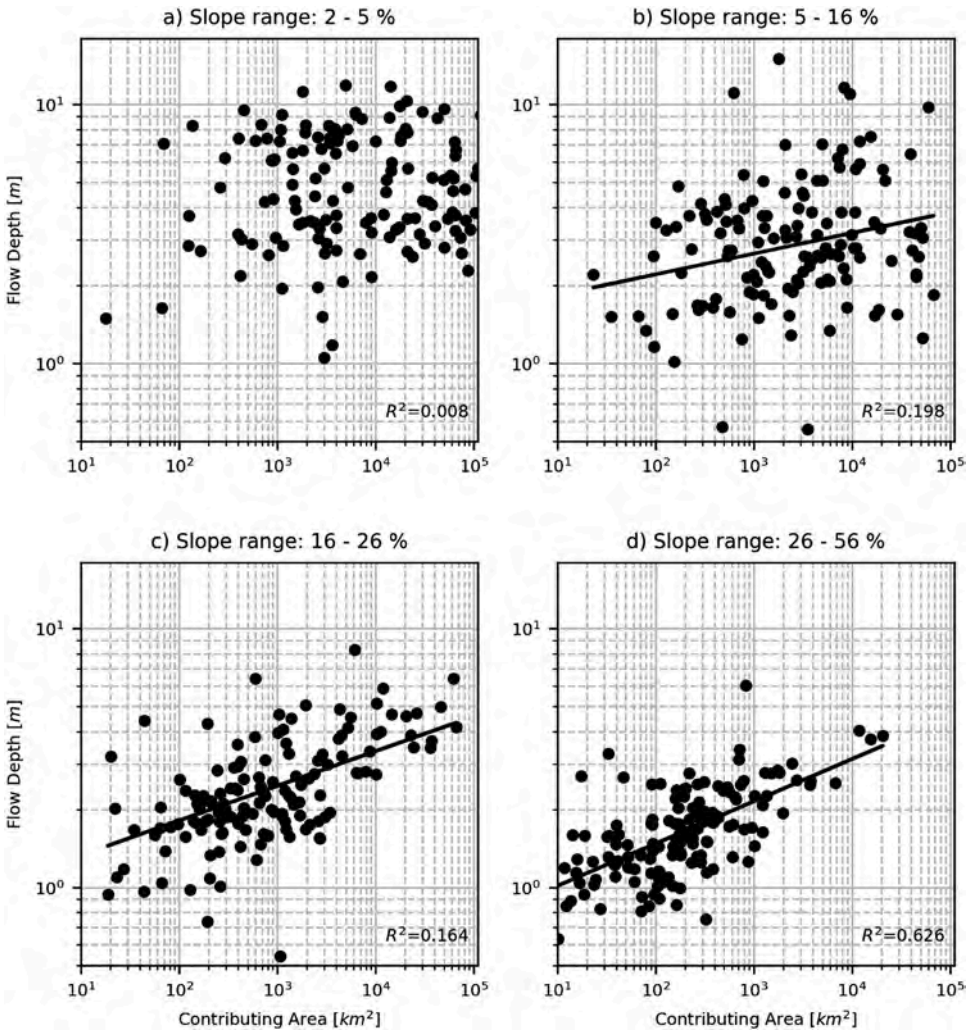

Fig. 6. Regression plots of the contributing area versus the 100-year flood stages changing ranges of sub-basins' slopes. Each circle represents the 100-year flow depths, the black lines represent the regression of the scaling law $\boldsymbol{d = aA^b}$. A trend line is not reported in Panel a) because of the low R^2 coefficient and high p-value (> 0.05).

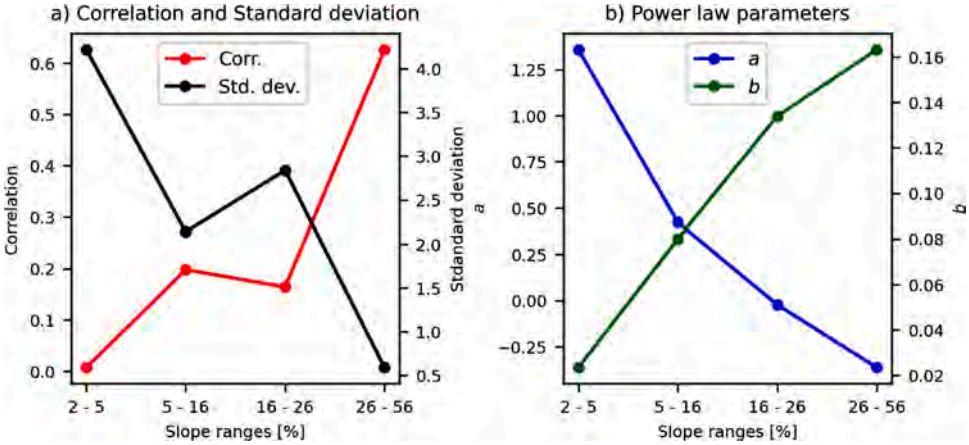

Fig. 7. Correlation coefficients –red- and standard deviation – black- (left panel), "a" – blue- and "b" – green- parameters of the regression laws as respect observed stage gages, varying sub-basins slope.

stream orders. Furthermore, the *a*-parameters generally decrease and the *b*-parameters increase as slope and rainfall increase for smaller Strahler stream orders (e.g. order 2–3). Higher stream order do not show clear patterns with varying slope and rainfall sets, and p-values are much higher than 0.05 (see Supplementary material). This could be due to the fact that the analysis for higher stream orders is affected by the presence of hydraulic control structures in the study area (see Supplementary material)

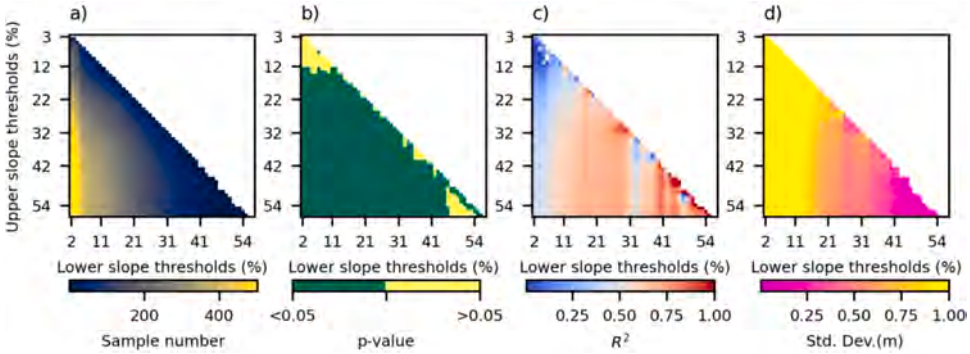

Fig. 8. Heatmaps of sample number (a), p-value with significance level of 0.05 (b), R2 (c), Standard deviation (d) related to the d-A regression law varying lower and upper slope ranges.

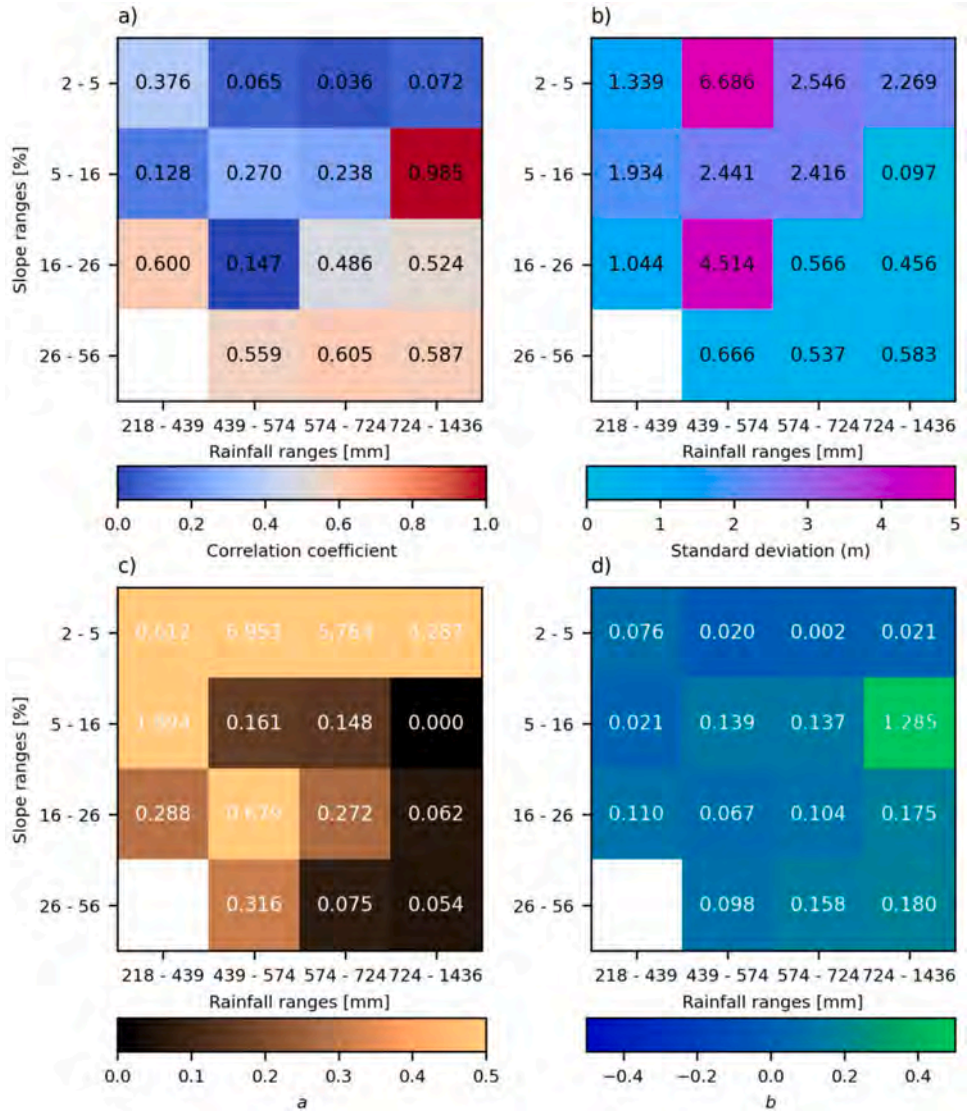

Fig. 9. Heatmaps of the correlation coefficients (top-left panel), standard deviation (top-right panel), "a" (bottom-left panel) and "b" (bottom-right panel) of the regression laws for each rainfall and slope range . White boxes correspond to no combinations of slope-rainfall ranges in the study area.

4.6. Comparison of the different regression models

Before comparing the performance of the regression models, an analysis of variance (ANOVA) of the different classes of the regression models were done to test if the classes belong to different populations and differences in results were not due to stochastic errors inside each class. The ANOVA analysis was performed variables of both contributing areas and 100-years flow depths. Table 3 shows the ANOVA results for the regression models described in Sections 4.3, 4.4, 4.5. Using a level of significance of 5% for all the regression models, Fisher-Snedecor (F-

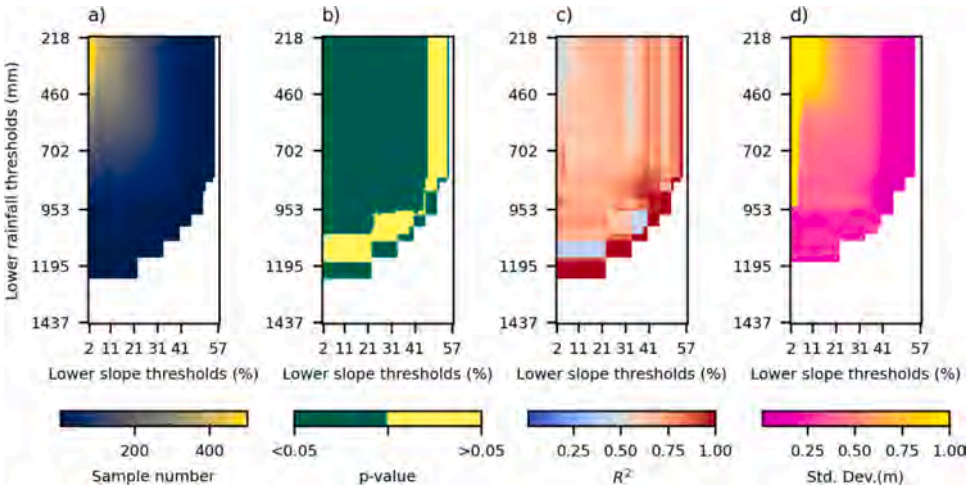

Fig. 10. Heatmaps of sample number (a), p-value (b), R^2 (c), Standard deviation (d) related to the d-A regression law varying lower slope and rainfall ranges.

values) and p-values reject the null hypothesis ($p < 0.05$), indicating statistical significant differences among classes.

We compared the results of three regression models that estimated flow depths associated with the 100-year recurrence interval. The three regression models included: a simple *d-A* regression illustrated in Section 4.1 (*M0*); a regression model with scaling parameters updated based on sub-basins' partial slope and annual rainfall (*M1*); and a regression model with scaling parameters updated based on sub-basins' stream orders, partial slope, and annual rainfall (*M2*).

Note that in stream orders where p-values were greater than 0.05 we assigned the regression parameters obtained with the closer stream order at the same slope and rainfall range. Based on root-mean-square-error values, results from both *M1* and *M2* demonstrated an improvement in flow depth estimation compared to *M0* (Table 4).

The selected case study is characterized by several flow control structures (e.g. dams, weirs) that affect almost all the analysed sub-basins. Flow control structures can have a negative influence on the regression model performances. Using the National Inventory of Dams (NID) dataset (USACE, 2015), we observed higher values of RMSE with the increase of the total regulation volumes of the flow control structures aggregated per stream orders (See Figure SM7 of the Supplementary Material).

4.7. GFPLAIN hydrogeomorphic floodplain refined parametrization adopting the proposed climate- and morphometry- varying scaling law

Furthermore, to explore whether the hydrogeomorphic floodplain identification algorithms can be improved by using flexible scaling parameters, we modified the GFPLAIN hydrogeomorphic model developed by Nardi et al. (2006, F. 2018) to automatically vary the parameterization of the scaling laws with the defined ranges of partial slopes and average annual rainfall of the drainage basins belonging to each stream of the computational domain (*M2*), and we compared the floodplain areas produced by updated GFPLAIN algorithm to standard flood hazard maps (FEMA, return period 100 years) using CSI and TP indices. We also compared the simulated floodplain areas identified using GFPLAIN without updated scaling parameters based on sub-basin slope and rainfall (*M0*). The CSI and TP values comparing the two hydrogeomorphic floodplain results to the standard flood hazard maps in each sub-basin where FEMA maps were available are showed in Fig. 12. Note that standard flood hazard maps are not expected to be perfectly aligned with results from the hydrogeomorphic floodplain models since the latter is aimed to delineate floodplain areas derived by the erosion and deposition processes occurring over millennial without considering recent anthropic modifications to rivers, such as levees, bridges, weirs and dams. Therefore, absolute values of CSI are not relevant, but relative values of CSI obtained for different hydrogeomorphic models can give information on their suitability, since standard flood maps are derived by hydrologic and hydraulic models that consider climate and morphometry of the study areas. Both the CSI and TP values for *M2* are respectively higher compared to values for M*0*, most notably TP values. This indicates that the hydrogeomorphic floodplain model can reduce the underestimation of the floodplain extension, confirming that parameterization of the *d-A* scaling law considering slope and rainfall ranges is able to delineate more accurate floodplain extensions.

A map of the hydrogeomorphic delineated floodplain dataset is showed in Fig. 13. Insets show a comparison with the GFPLAIN250m dataset (Nardi et al., 2019) in areas with different climate and morphometry. Note that *M2* and GFPLAIN datasets are characterized by different resolution (respectively 30 and 250 m); however, different floodplain extents illustrated in the 5 insets of Fig. 13 are mostly due to the different *d-A* scaling law parameterization that led to different flow depths distributions.

5. Discussion

The proposed analysis demonstrated that partial sub-basins slope (PSL) and partial average annual rainfall (APR) are among the most influential morphometric and climatic factors in the applicability of the depth-contributing area (*d-A*) regression laws. PSL and PAR are also suitable for performing fast large-scale analysis in GIS environment since they can be easily determined with a simple zonal statistic using available datasets for sub-basin boundaries, slope, and rainfall. On the other hand, variables such TCR, TSL and TAR require a much higher computational effort. The mean basin slope (strongly correlated with the partial sub-basin slope as showed in Figure SM2 of the Supplementary Material) has been shown to be one of the most relevant morphological correlated with inundation extent (Jafarzadegan and Merwade, 2017). And, processes of channel/floodplain morphology, such as sediment dynamics, are related to annual precipitation (Langbein and Schumm, 1958). Similar regression results in terms of scaling law parameters and performance metrics were obtained considering TSL and TAR ranges (See Section 1.6 of the Supplementary Material) confirming that PSL and PAR for sub-basins with at least 10 km^2 of partial area can be considered adequate variables for disaggregating scaling laws parameterizations.

When *d-A* regression law is disaggregated for different ranges of the above-mentioned parameters, low values of Person's correlation coefficient are obtained for sub-basins with small slope ranges. This behavior underlines the strong limitation of using scaling laws in dry and flat areas, were basin gradients are unable to generate the sufficient energy

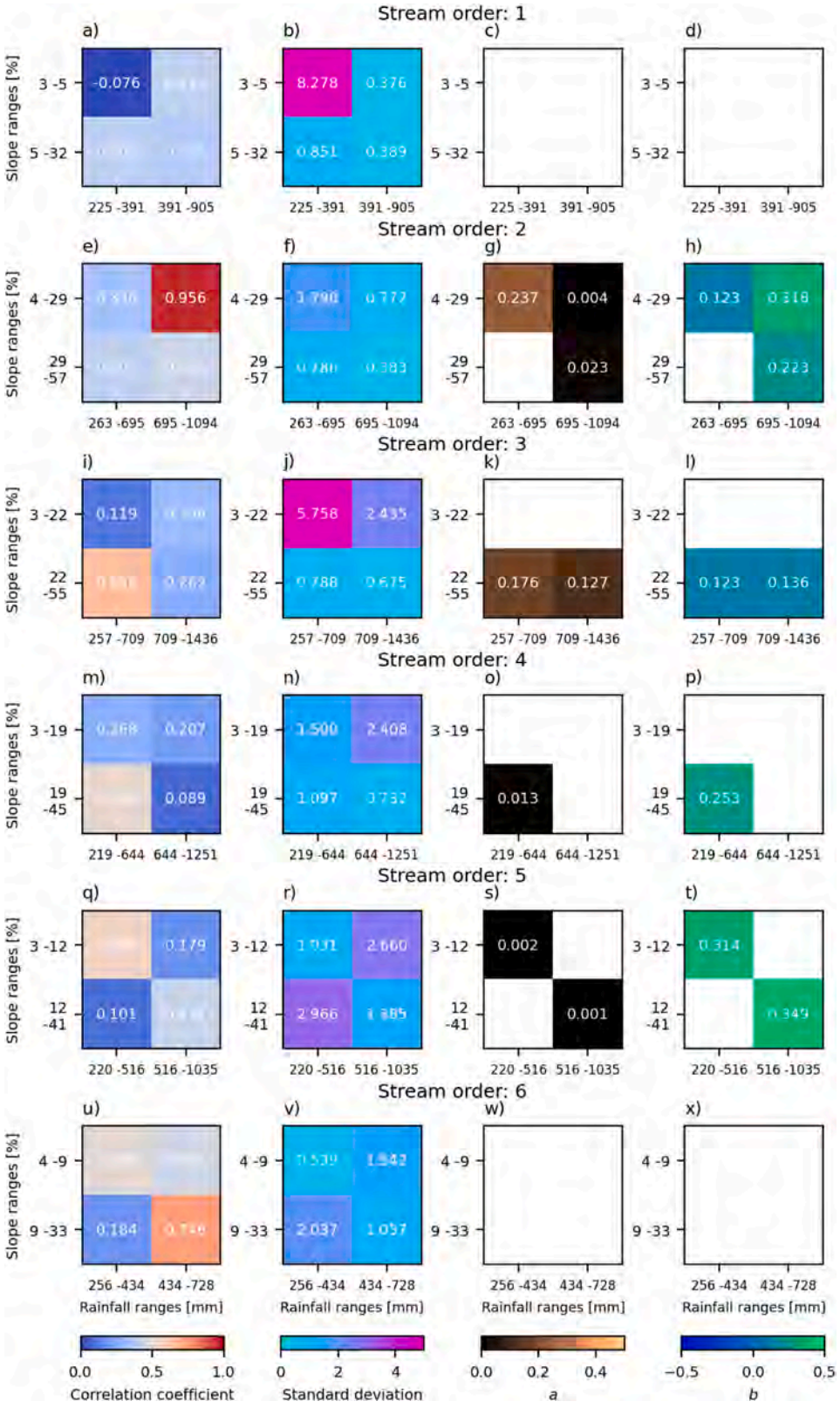

Fig. 11. Heatmaps of the correlation coefficients (1° column), Standard deviation (2° column), "a" and "b" scaling law parameters (3° and 4° columns) derived from the d-A regression distinguishing stream orders, slope, and rainfall ranges. White boxes of a and b parameters indicate that p-values tests are not satisfied.

to increase the flow peak with the increasing of contributing areas. On the other hand, *d-A* scaling law regressions give higher correlation and lower standard deviation errors average annual rainfall increases, regardless of the slope range. This indicates that the effectiveness of scaling laws in steep basins is weakly depending on the dryness of the studied areas.

The adopted GFPLAIN model was previously applied using constant parametrization of the scaling law producing consistent results of

Table 3
Results of the analysis of variance (ANOVA) for the three regression models based on contributing areas and 100-years flow depths. Note that 2 classes from the regression model with 16 classes of slope and rainfall ranges (M1) have been excluded because of their small sample sizes.

Regression model	Contributing area		100-years flow depths	
	F-value	p-value	F-value	p-value
Regression varying slope	24.62	5.81E-15	45.69	2.18E-26
Regression varying slope and rainfall (M1)	11.46	3.07E-15	13.52	9.42E-18
Regression varying slope, rainfall and stream orders (M2)	1.81	2.39E-02	19.51	3.57E-48

Table 4
Comparison of the Root Mean Squared Errors of three regression models: M0 (Simple d-A regression illustrated in Section 4.1), M1 (Regression tailored considering sub-basins' partial slope and annual rainfall), M2 (Regression tailored considering sub-basins' stream orders, partial slope and annual rainfall).

Regression models	RMSE (m)
M0	1.11
M1	0.97
M2	0.95

floodplain delineations maps (Nardi et al., 2019; Di Baldassarre et al., 2020) and demonstrated the model can consistently identify floodplain surfaces created by fluvial erosion/deposition processes at a global scale regardless of the climatic and morphometric basins settings. Nevertheless, when evaluating the GFPLAIN results at smaller scales, it is clear that inaccuracies may be present, especially where the topography-based principle does not hold as it may happen in arid regions and in river basins where Hortonian surface runoff are not the major drivers of fluvial shaping dynamics. As a result, this study provided an improvement of the GFPLAIN model by suggesting a regionalized *d-A* scaling law that takes into account the morpho-climatic conditions. Results confirm that the validity or range of inapplicability of the scaling law. In particular, our results suggest the following range of validity for the selected study basins:

- Sub-basins slope higher than 5%
- Average annual rainfall higher than 570 mm.

Moreover, for the scaling laws corresponding to 100-years return period depths, the following regionalized scaling law parametrization may be applied:

- *a* parameter varies from 1.5 (slopes lower than 16%) to 0.054 (slopes greater than 26% and average annual rainfall higher than 725 mm).
- *b* parameter varies from 0.05 (slopes lower than 16%) to 1.18 (slopes greater than 26% and average annual rainfall higher than 725 mm).

Since these parameters ranges proved to be effective at improving a hydrogeomorphic model with a widely available DEM (NASADEM, Crippen et al., 2016), they can be adopted in other river basins with similar ranges of slopes and rainfall.

We recognize that water management infrastructure, such as dams, diversions, and levees can influence floodplain connectivity and flood recurrence calculations. Further investigations should be conducted to understand how basins with flow control structures can influence *d-A* scaling law regressions compared to unregulated river basins. This work demonstrated some influence of reservoir storage on parameterization within stream orders (see Figure SM7 in the Supplementary Material), but further comparisons should be carried out. Specifically, a comparison of scaling law parameterizations of the analysed case study with other unregulated river basins with same ranges of basin slope and rainfall are needed.

The outcomes of the proposed analysis may pave the way for improving large scale floodplain delineation datasets, such as GFPLAIN, considering morphometric and climatic factors that are freely available at global scale. Moreover, these outcomes can support improvements of other floodplain delineation methods based on scaling laws (C. Samela et al., 2017c) or refinement of datasets aimed to provide channel depth estimations for large scale (e.g. continental or global) flood models (Andreadis et al., 2013).

6. Conclusions

In this paper we investigated the applicability and the parameterization of contributing areas (*A*) -floodplain flow depths (*d*) scaling laws for different ranges of partial sub-basins slope and average annual rainfall to improve a hydrogeomorphic floodplain delineation model. Partial sub-basin slope and mean annual rainfall were chosen after a preliminary analysis on the most influential factor of several basins' parameters on the effectiveness of *d-A* regression laws. As case studies, we selected eleven river basins in the United States characterized by high variability of slopes, elevations and average annual rainfall. The main conclusions derived by the analyses are summarized below:

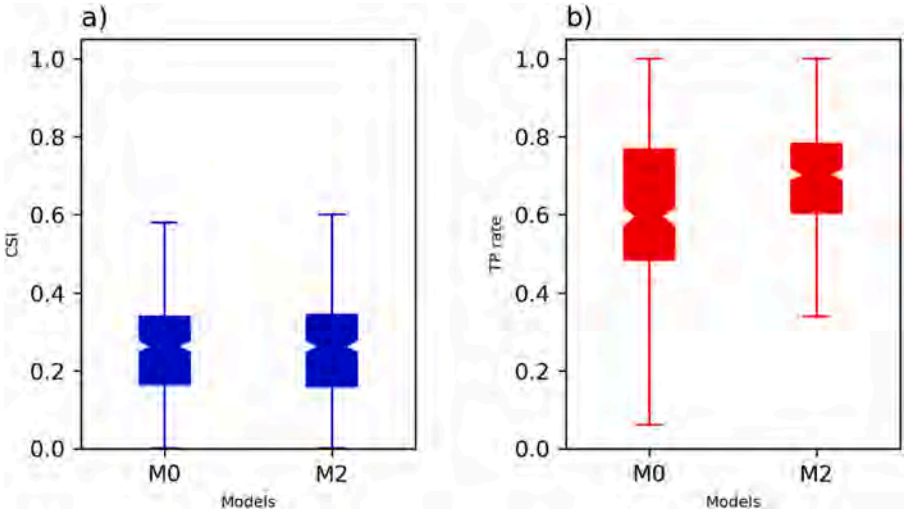

Fig. 12. Boxplots of the Critical Success Index (CSI, panel a) and True Positive (TP, panel b) values related to the comparison between the FEMA 100 years flood maps extension and the floodplain extensions derived by the standard hydrogeomorphic model parameterized (M0- Section 4.1), and the new one tailored for considering, stream orders, partial mean slopes and annual rainfall distributions (M2- Section 4.5). The boxes extend from the lower to upper quartile values of the data, with the central taper line at the median. The whiskers extend from the box to show the range of the data.

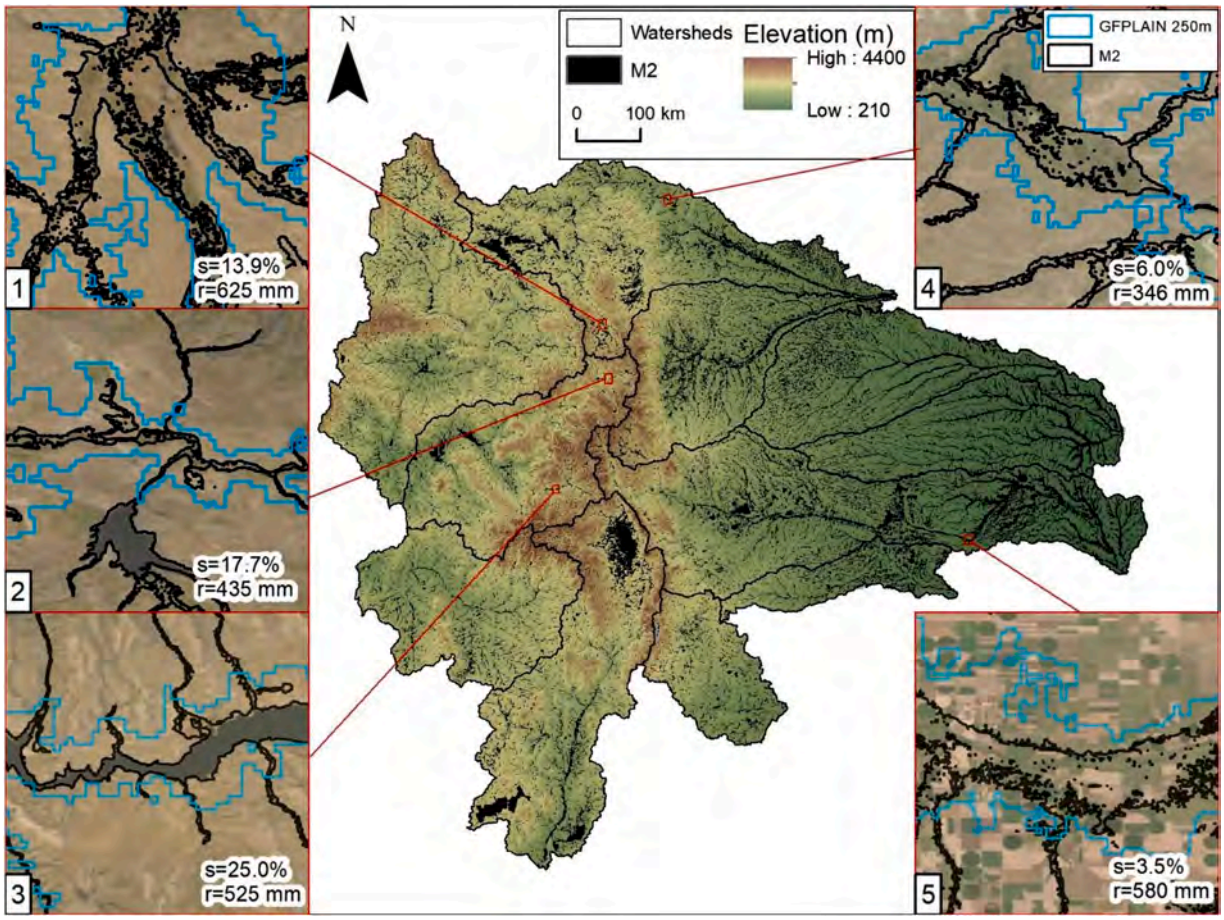

Fig. 13. Map of the floodplain dataset M2 (derived in this work by the application of the d-A regression with the NASADEM tailored considering sub-basins' stream orders, partial slope and annual rainfall – black filled polygon) with the GFPLAIN 250 m dataset (derived globally by Nardi et al., 2019 applying the d-A regression with constant parameterization– blue bordered polygon). In the right bottom corner of the 5 insets, "s" is subbasins mean slope (%) and " r" is the subbasin average annual rainfall (mm).

- Low correlation coefficients related to the regression laws were observed for sub-basins characterized by mean slopes lower than 5%.
- For the sub-basins with mean slopes higher than 5%, the scaling law parameters are correlated to intervals of sub-basins slopes; specifically the a parameter tends decrease, while the exponent b tend to increase with the increasing of mean slope intervals. For the same mean slope ranges, the a parameter weakly tends decrease, while the exponent b and the correlation coefficient tend to increase with the increasing of average annual rainfall.
- A hydro-geomorphic floodplain model based on the *d-A* scaling law formula application has been improved considering parameterizations for different stream orders and intervals of slopes and average annual rainfall. The modified model provided better results in terms of floodplain extensions compared to the standard hazard flood maps as respect to the standard regression model.

Further investigations for improving the hydrogeomorphic model are required in different climatic areas and in flat and dry areas where scaling laws have poor correlations and where alternative approaches could be considered.

Declaration of Competing Interest

The authors declare that they have no known competing financial interests or personal relationships that could have appeared to influence the work reported in this paper.

Supplementary materials

Supplementary material associated with this article can be found, in the online version, at doi:10.1016/j.advwatres.2021.104078.

References

Andreadis, K.M., Schumann, G.J.P., Pavelsky, T., 2013. A simple global river bankfull width and depth database. Water Resour. Res. (10), 49, 10.1002/wrcr.20440.
Annis, A., Nardi, F., Morrison, R.R., Castelli, F., 2019. Investigating hydrogeomorphic floodplain mapping performance with varying DTM resolution and stream order. Hydrol. Sci. J. 64 (5), 525–538. Taylor & Francis10.1080/02626667.2019.1591623.
Baldassarre, G.Di, Nardi, F., Annis, A., Odongo, V., Rusca, M., Grimaldi, S., 2020. Brief communication: comparing top-down and bottom-up paradigms for global flood hazard mapping. Nat. Hazards Earth Syst. Sci. Discuss. 2016, 1–6, 10.5194/nhess-2019-418.
Beechie, T.J., Liermann, M., Pollock, M.M., Baker, S., Davies, J., 2006. Channel pattern and river-floodplain dynamics in forested mountain river systems. Geomorphology 78 (1–2), 10.1016/j.geomorph.2006.01.030.
Bhowmik, N.G., 1984. Hydraulic geometry of floodplains. J. Hydrol. 10.1016/0022-1694(84)90221-X.
Bourke, M.C., Pickup, G., 1999. Fluvial form and variability in arid Central Australia. Varieties of Fluvial Form.
Chorley, R.J., 1957. Climate and morphometry. J. Geol. 65 (6), 10.1086/626468.
Chow, V.Te., 1965. Handbook of applied hydrology. Int. Assoc. Sci. Hydrol. Bull. 10 (1), 10.1080/02626666509493376.
Clubb, F.J., Mudd, S.M., Milodowski, D.T., Valters, D.A., Slater, L.J., Hurst, M.D., Limaye, A.B., 2017. Geomorphometric delineation of floodplains and terraces from objectively defined topographic thresholds. Earth Surf. Dyn. 5 (3), 10.5194/esurf-5-369-2017.
Costa, J.E., 1987. Hydraulics and basin morphometry of the largest flash floods in the conterminous United States. J. Hydrol. 93 (3–4), 10.1016/0022-1694(87)90102-8.
Crippen, R., Buckley, S., Agram, P., Belz, E., Gurrola, E., Hensley, S., Kobrick, M., et al., 2016. Nasadem global elevation model: methods and progress. Int. Arch.

Photogramm. Remote Sens. Spat. Inf. Sci. - ISPRS Arch. 10.5194/isprsarchives-XLI-B4-125-2016.
Daly, C., Bryant, K., 2013. The PRISM climate and weather system - an introduction. Prism Clim. Gr.
Dodov, B.A., Foufoula-Georgiou, 2006. Floodplain morphometry extraction from a high-resolution digital elevation model: a simple algorithm for regional analysis studies. IEEE Geosci. Remote Sens. Lett. 10.1109/LGRS.2006.874161.
Dodov, B., Foufoula-Georgiou, E., 2004a. Generalized hydraulic geometry: insights based on fluvial instability analysis and a physical model. Water Resour. Res. 10.1029/2004WR003196.
Dodov, B., Foufoula-Georgiou, E., 2004b. Generalized hydraulic geometry: derivation based on a multiscaling formalism. Water Resour. Res. 40 (6), 1–22, 10.1029/2003WR002082.
Dodov, B., Foufoula-Georgiou, E., 2005. Fluvial processes and streamflow variability: interplay in the scale-frequency continuum and implications for scaling. Water Resour. Res. 41 (5), 1–18, 10.1029/2004WR003408.
Döll, P., Fiedler, K., Zhang, J., 2009. Global-scale analysis of river flow alterations due to water withdrawals and reservoirs. Hydrol. Earth Syst. Sci. 13 (12), 10.5194/hess-13-2413-2009.
Dunkerley, D.L., 1992. Channel geometry, bed material, and inferred flow conditions in ephemeral stream systems, barrier range, western N.S.W. Australia. Hydrol. Process. 10.1002/hyp.3360060404.
Ferguson, R.I., 1986. Hydraulics and hydraulic geometry. Prog. Phys. Geogr. 10.1177/030913338601000101.
Galloway, W.E., Hobday, D.K., 1996. Terrigenous clastic depositional systems. Terrigenous Clastic Depos. Syst. 10.1007/978-3-642-61018-9.
Graf, W.L., 1988. Definition of flood plains along arid-region rivers. Flood Geomorphol.
Gravelius, H., 1914. *Flusskunde*. GJ göschen.
Gregory, K.J., Walling, K.J., 1968. The variation of drainage density within a catchment. Int. Assoc. Sci. Hydrol. Bull. 13 (2), 10.1080/02626666809493583.
Gurnell, A.M., Bertoldi, W., Corenblit, D., 2012. Changing river channels: the roles of hydrological processes, plants and pioneer fluvial landforms in humid temperate, mixed load, gravel bed rivers. Earth-Sci. Rev. 111 (1–2), 10.1016/j.earscirev.2011.11.005.
Hastie, T.J., Tibshirani, R.J., 1990. Generalized Additive Models, Monographs on Statistics and Applied Probability 43. Chapman Hall, 10.1016/j.csda.2010.05.004.
Hickin, E.J., 2009. River Channel Changes: retrospect and Prospect. Modern and Ancient Fluvial Systems, 10.1002/9781444303773.ch5.
Horton, R.E., 1932. Drainage-basin characteristics. Eos, Trans. Am. Geophys. Union 13 (1), 10.1029/TR013i001p00350.
Horton, R.E., 1945. Erosional development of streams and their drainage basins; Hydrophysical approach to quantitative morphology. Bull. Geol. Soc. Am. 56 (3), 10.1130/0016-7606(1945)56[275:EDOSAT]2.0.CO;2.
Jafarzadegan, K., Merwade, V., 2017. A DEM-based approach for large-scale floodplain mapping in ungauged watersheds. J. Hydrol. 10.1016/j.jhydrol.2017.04.053.
Jenson, S.K., Domingue, J.O., 1988. Extracting topographic structure from digital elevation data for geographic information system analysis. Photogrammetric Engineering and Remote. Photogramm. Eng. Remote Sensing.
Knighton, A.D., Nanson, G.C., 1993. Anastomosis and the continuum of channel pattern. Earth Surf. Process. Landforms, 10.1002/esp.3290180705.
Knighton, D., 2014. Fluvial forms and processes: a new perspective. Fluv. Forms Process. A New Perspect. 10.4324/9780203784662.
Langbein, W.B., Schumm, S.A., 1958. Yield of sediment in relation to mean annual precipitation. Eos, Trans. Am. Geophys. Union, 10.1029/TR039i006p01076.
Leopold, L.B., Maddock, T.J., 1953. The hydraulic geometry of stream channels and some physiographic implications. Geol. Surv. Prof. Pap. 252.
Leopold, L.B., Wolman, M.G., 1970. River channel patterns. Rivers and River Terraces, 10.1007/978-1-349-15382-4_8.
Lurtz, M.R., Morrison, R.R., Gates, T.K., Senay, G.B., Bhaskar, A.S., Ketchum, D.G., 2020. Relationships between riparian evapotranspiration and groundwater depth along a semiarid irrigated river valley. Hydrol. Process. 34 (8), 10.1002/hyp.13712.
Manfreda, S., Nardi, F., Samela, C., Grimaldi, S., Taramasso, A.C., Roth, G., Sole, A., 2014. Investigation on the use of geomorphic approaches for the delineation of flood prone areas. J. Hydrol. 10.1016/j.jhydrol.2014.06.009.
Manfreda, S., Samela, C., Gioia, A., Consoli, G.G., Iacobellis, V., Giuzio, L., Cantisani, A., et al., 2015. Flood-prone areas assessment using linear binary classifiers based on flood maps obtained from 1D and 2D hydraulic models. Nat. Hazards, 10.1007/s11069-015-1869-5.
Melton, M.A., 1957. An analysis of the relations among elements of climate, surface properties, and geomorphology; office of naval research technical report No. 11. Off. Nav. Res. Tech. Rep.
Merritt, D.M., Wohl, E.E., 2003. Downstream hydraulic geometry and channel adjustment during a flood along an ephemeral, arid-region drainage. Geomorphology 52 (3–4), 165–180, 10.1016/S0169-555X(02)00241-6.
Miller, O.M., Summerson, C.H., 1960. Slope-zone maps. Geogr. Rev. 50 (2), 10.2307/211507.
Montgomery, D.R., Buffington, J.M., 1997. Channel-reach morphology in mountain drainage basins. Bull. Geol. Soc. Am. 109 (5), 10.1130/0016-7606(1997)109<0596:CRMIMD>2.3.CO;2.
Morrison, R.R., Bray, E., Nardi, F., Annis, A., Dong, Q., 2018. Spatial relationships of levees and wetland systems within floodplains of the Wabash Basin, USA. J. Am. Water Resour. Assoc. 54 (4), 934–948, 10.1111/1752-1688.12652.
Mueller, J.E., 1968. An introduction to the hydraulic and topographic sinuosity indexes. Ann. Assoc. Am. Geogr. 58 (2), 10.1111/j.1467-8306.1968.tb00650.x.
Nadler, C.T., Schumm, S.A., 1981. Metamorphosis of south platte and arkansas rivers, eastern colorado. Phys. Geogr. 10.1080/02723646.1981.10642207.
Nardi, F., Annis, A., Baldassarre, G.Di, Vivoni, E.R., Grimaldi, S., 2019. GFPLAIN250m, a global high-resolution dataset of earth's floodplains. Sci. Data 6, 1–6. The Author(s) 10.1038/sdata.2018.309.
Nardi, F., Biscarini, C., Francesco, S.Di, Manciola, P., Ubertini, L., 2013. Comparing a large-scale dem-based floodplain delineation algorithm with standard flood maps: the tiber river basin case study. Irrig. Drain. 10.1002/ird.1818.
Nardi, F., Morrison, R.R., Annis, A., Grantham, T.E., 2018. Hydrologic scaling for hydrogeomorphic floodplain mapping: insights into human-induced floodplain disconnectivity. River Res. Appl. 10.1002/rra.3296.
Nardi, F., Vivoni, E.R., Grimaldi, S., 2006. Investigating a floodplain scaling relation using a hydrogeomorphic delineation method. Water Resour. Res. 42 (9) n/a-n/a10.1029/2005WR004155.
Parsons, T., 1994. Book reviews : Cooke, R.U., Warren, A. and Goudie, A.S. 1993: Desert geomorphology. UCL Press, London viii + 526 pp. £75.00 cloth, £24.95 paper. ISBN: 1 857280164. *Prog. Phys. Geogr. Earth Environ.*,. doi:10.1177/030913339401800314.
Samela, C., Manfreda, S., Troy, T.J., 2017a. Dataset of 100-year flood susceptibility maps for the continental U.S. derived with a geomorphic method. Data Br, 10.1016/j.dib.2017.03.044.
Samela, C., Troy, T.J., Manfreda, S., 2017b. Geomorphic classifiers for flood-prone areas delineation for data-scarce environments. Adv. Water Resour. 10.1016/j.advwatres.2017.01.007.
Samela, C., Troy, T.J., Manfreda, S., 2017c. Geomorphic classifiers for flood-prone areas delineation for data-scarce environments. Adv. Water Resour. 102, 13–28. Elsevier Ltd10.1016/j.advwatres.2017.01.007.
Sangwan, N., Merwade, V., 2015. A Faster and Economical Approach to Floodplain Mapping Using Soil Information. J. Am. Water Resour. Assoc. 10.1111/1752-1688.12306.
Scheel, K., Morrison, R.R., Annis, A., Nardi, F., 2019. Understanding the large-scale influence of levees on floodplain connectivity using a hydrogeomorphic approach. J. Am. Water Resour. Assoc. 10.1111/1752-1688.12717.
Schumm, S.A., 1985. Patterns of alluvial rivers. Annu. Rev. Earth Planet. Sci. Vol. 13, 10.1146/annurev.earth.13.1.5.
Seaber, P.R., Kapinos, F.P., Knapp, G.L., 1987. Hydrologic unit maps (USA). US Geol. Surv. Water-Supply Pap. 10.3133/wsp2294.
Sechu, G.L., Nilsson, B., Iversen, B.V., Greve, M.B., Børgesen, C.D., Greve, M.H., 2020. A stepwise GIS approach for the delineation of river valley bottom within drainage basins using a cost distance accumulation analysis. Hydrol. Earth Syst. Sci. July10.5194/hess-2020-361.
Stout, J.C., Belmont, P., 2014. TerEx toolbox for semi-automated selection of fluvial terrace and floodplain features from lidar. Earth Surf. Process. Landforms 39 (5), 10.1002/esp.3464.
Strahler, A.N., 1952. Dynamic basis of geomorphology. Bull. Geol. Soc. Am. 63 (9), 10.1130/0016-7606(1952)63[923:DBOG]2.0.CO;2.
Tooth, S., 2000. Process, form and change in dryland rivers: a review of recent research. Earth Sci. Rev. 51 (1–4), 67–107, 10.1016/S0012-8252(00)00014-3.
Tooth, S., 2009. Downstream changes in floodplain character on the northern plains of arid central Australia. Fluv. Sedimentol. VI 93–112, 10.1002/9781444304213.ch8.
Trabucco, A., Zomer, R.J., 2018. Global aridity index and potential evapo-transpiration (ET0) climate database v2. Clim. Database v2. CGIAR Consort. Spat. (CGIAR-CSI). https://doi.org/10.6084/m9.figshare.7504448.v3.
U.S. Water Resources Council. Hydrology Committee., 1981. Guidelines for determining flood flow frequency. Bulletin 17B. US Water Resour. Counc.
UNEP., 1997. World Atlas of Desertification 2ED. United Nations Environ. Program.
USACE., 2015. National inventory of dams. CorpsMap.
Wohl, E., Lininger, K.B., Baron, J., 2017. Land before water: the relative temporal sequence of human alteration of freshwater ecosystems in the conterminous United States. Anthropocene, 10.1016/j.ancene.2017.05.004.
Wolman, M.G., Miller, J.P., 1960. Magnitude and frequency of forces in geomorphic processes. J. Geol. 68 (1), 10.1086/626637.
Zomer, R.J., Trabucco, A., Bossio, D.A., Verchot, L.V., 2008. Climate change mitigation: a spatial analysis of global land suitability for clean development mechanism afforestation and reforestation. Agric. Ecosyst. Environ. 10.1016/j.agee.2008.01.014.